The final authenticated version is available online at: https://doi.org/10.7567/1347-4065/ab0ba0

Photoconductivity of Er-doped InAs quantum dots embedded in strain-relaxed InGaAs layers with 1.5 μm cw and pulse excitation

Keisuke Murakumo*, Yuya Yamaoka, Naoto Kumagai, Takahiro Kitada, and Toshiro Isu

Center for Frontier Research of Engineering, Institute of Technology and Science, Tokushima University, Tokushima 770-8506, Japan

We fabricated a photoconductive antenna structure utilizing Er-doped InAs quantum dot layers embedded in strain-relaxed $In_{0.35}Ga_{0.65}As$ layers on a GaAs substrate. Mesa-shaped electrodes for the antenna structure were formed by photolithography and wet etching in order to suppress its dark current. We measured the photocurrent with the excitation of ~1.5 μm cw and femtosecond pulse lasers. Compared with the dark current, the photocurrent was clearly observed under both cw and pulse excitation conditions and almost linearly increased with increasing excitation power in a wide range of magnitudes from 10 W/cm^2 to 10 MW/cm^2 order.

1. Introduction

Photoconductive (PC) antennas are important devices for detecting and emitting THz waves.[1–6] The optical gating operation of a PC antenna is based on the generation of photocarriers by the excitation of a femtosecond (fs) pulse laser and its relaxation. A suitable material for a PC antenna requires the characteristic properties of ultrafast photocarrier relaxation, a low dark current (high sheet resistance), and a larger photocurrent than dark current. Low-temperature-grown (LT) GaAs and LT InGaAs on an InP substrate obtained by molecular beam epitaxy (MBE) are well known as conventional and commercially available materials for a PC antenna.[7–13] For LT GaAs, the wavelength of the gating light is ~0.8 μm, which corresponds to the absorption wavelength of bulk GaAs. However, the typical source for a wavelength of ~0.8 μm is a Ti:sapphire laser, which is an expensive and unconventional system that is difficult to handle. Therefore, LT InGaAs, whose absorption wavelength is ~1.5 μm, has been studied in order to use 1.5-μm-band fiber lasers, which are more conventional and compact sources than Ti:sapphire lasers. However, it is difficult for LT InGaAs to achieve a high sheet resistance of ~MΩ/sq due to the residual electron concentration in undoped

*E-mail:c501438005@tokushima-u.ac.jp

InGaAs.[12–14] Although many attempts, such as introducing ErAs or a superlattice of InAlAs into the InGaAs layer, have been made to improve the sheet resistance and characteristics of a PC antenna,[15–19] these materials were designed focusing only on operating at the 1.5 μm band. On the other hand, studies on the operation of PC antennas for various wavelengths for 1.0-1.2 μm bands were reported .[20–23] In future, PC antennas operating with various wavelengths are expected with the further progress of fs pulse lasers with a wider range of wavelengths.

Recently, we proposed utilizing quantum dot (QD) structures for a PC antenna.[24,25] Compared with bulk materials such as LT GaAs and LT InGaAs, QD structures may allow a more flexible design of the PC antenna such as control of the absorption wavelength by optimization of the growth conditions of QDs. The realization of PC antennas operating with various wavelengths is expected due to this potential in consideration of the recent progress of pulse lasers. In our previous studies, we reported the characteristic properties of InAs QDs embedded in strain-relaxed $In_{0.35}Ga_{0.65}As$ layers. The QDs show absorption in the optical communication band of 1.55 μm and ultrafast photocarrier relaxation (18 ps).[26] The longer absorption wavelength than that of usual InAs/GaAs QDs ($\sim$1.2 μm)[27–32] or InAs/InGaAs QDs ($\sim$1.3μm)[33–35] is due to the lowered potential height and reduced strain in InAs QDs. The ultrafast photocarrier relaxation compared with that in usual InAs QDs on GaAs[36,37] comes from the recombination at non-radiative centers induced by crystal defects due to the lattice mismatch. Furthermore, faster relaxation with a relaxation time as short as $\sim$1.6 ps was achieved by the direct doping of erbium (Er) to InAs QD layers.[38,39] Due to these optical properties, Er-doped InAs QDs embedded in strain-relaxed $In_{0.35}Ga_{0.65}As$ layers are expected to be applied to PC antennas operating with a gating light of 1.55 μm on GaAs substrates. Generally, the density of states of QDs is smaller than that of a bulk material, which may cause saturable absorption for a lower power excitation than for the case of the bulk. Saturable absorption results in the degradation of linear absorption. However, the smaller density of states in a QD system can be compensated for by epitaxial growth techniques such as the stacking of QD layers and increasing the QD density.

In this work, we fabricated a photoconductive antenna structure utilizing Er-doped InAs QDs embedded in strain-relaxed $In_{0.35}Ga_{0.65}As$ layers with a mesa shape by photolithography and wet etching. We obtained the current-voltage (I-V) characteristics and the excitation power dependence of the photocurrent with the excitation of 1.5 μm cw and pulse lasers.

2. Experiment

The stacking structure of InAs QDs layers shown in Fig. 1 was grown on a semi-insulating GaAs (001) substrate by MBE. Following the growth of a 400 nm GaAs buffer layer at 630 °C , the substrate temperature was lowered to 430 °C and an $In_{0.35}Al_{0.65}As$ layer with 20 nm thickness was grown. Relaxation of the lattice strain was induced in the $In_{0.35}Al_{0.65}As$ layer. The coverage of the subsequently grown InAs QD layer on the $In_{0.35}Ga_{0.65}As$ layer was 3.4 ML, which was grown at 430 °C at a rate of 0.35 μm/h. The QD density per layer was $\sim 10^{11}$ cm^{-2}. The thickness of $In_{0.35}Ga_{0.65}As$ spacer layer between InAs QD layers was 20 nm. Er was directly irradiated only on the InAs QD layer. The sheet density of Er per QD layer was $\sim 2.7 \times 10^{13}$ cm^{-2}.[38] The obtained sheet resistance was 8.3 MΩ/sq from the van der Pauw method.

A typical dipole antenna pattern was drawn on the as-grown surface by photolithography. The schematic pattern is shown in Fig. 2. Ti/Au (5 nm/100 nm) electrodes were deposited on the sample surface to form an ohmic contact by vacuum deposition. After the deposition of antenna electrodes, the pattern for mesa formation was drawn around the deposited electrodes by photolithography. The area surrounding the electrodes except for the antenna gap centered at the electrodes was etched to 1.3 μm depth from the sample surface by wet etching using a mixed solution consisting of phosphoric acid, hydrogen peroxide, and water (1:1:6). The depth is enough to completely remove the epitaxial layer with a the total thickness of 0.8 μm. A schematic illustration of the fabrication process and an enlarged image of the antenna gap with the mesa formation are shown in Fig. 3. The width of the antenna gap was 4.4 μm, which is smaller than the designed value of 6 μm. To verify the effect of the mesa formation, the resistance between the electrodes was compared before and after the formation of mesa-shaped electrodes.

I-V characteristics and the power dependence of the photocurrent were measured for the antenna structure with the mesa-shaped electrodes under dark and excited conditions. The excitation source was a cw semiconductor laser and an fs pulse laser of 1.5 μm. Figure 4 shows a schematic illustration of the setup for photocurrent measurement. A pulse laser of $\sim$1.5 μm was produced by an optical parametric oscillator (OPO) pumped by a Ti:sapphire laser with a repetition rate of 80 MHz. The pulse width obtained by the OPO is 100 fs. For the excitation by the cw and pulse lasers, the size of the focused spot was $\sim$70 and $\sim$90 μm, respectively. Photocurrent was measured

with a bias voltage from -1 to +1 V using a source meter (Keithley 2450). Note that the measured photocurrent is a time-averaged value for the case of excitation by the pulse laser. Therefore, we consider that the peak value of the photocurrent corresponds to the peak power and compare the peak photocurrent with that for the cw excitation.

3. Results and discussion

Figure 5 shows the obtained I-V characteristics of the dark current with and without the formation of mesa-shaped electrodes. Without the mesa formation, the measured resistance was 22 KΩ, while the resistance with the mesa formation was 2.9 MΩ. From the result for the sheet resistance, the estimated resistance between the electrodes over the total antenna length of 5 μm, as shown in Fig. 5, is 33 KΩ. Thus, the low resistance between the electrodes may be due to the flow of the dark current for the whole length of the antenna. Also, the resistance of 2.9 MΩ between the mesa-shaped electrodes is consistent with the estimated value for the antenna gap obtained from the sheet resistance, which indicates that the dark current was ideally suppressed by the formation of the mesa-shaped electrodes without any passivation treatment with the as-etched side wall.

Figure 6 shows the obtained I-V characteristics under dark current and excitation of 25 mW for the cw and pulse excitation with a bias voltage between -1 and +1 V. In both cases, linear I-V characteristics were observed, which indicates the formation of an ohmic contact.

Figure 7 shows the excitation power dependence of the measured current from 0 to 50 mW at a bias voltage of +1 V in the case of the pulse excitation. Compared with the dark current, the measured current was clearly observed and linearly increased as the excitation power increased.

Here, we consider the peak value of the photocurrent corresponding to the peak power for the pulse excitation for comparison with the case of cw excitation. The peak power of the pulse laser is

$$P_{\mathrm{peak}} = P \times \frac{t_{\mathrm{p}}}{t_{\mathrm{d}}}, \tag{1}$$

where P_{peak} and P is peak laser power and excitation power, respectively. t_{d} and t_{p} are the pulse duration (100 fs) and pulse repetition time (12.5 ns), respectively. The photocurrent flows as a pulselike current because the rise and decay times of the photocurrent are much shorter than the repetition time of the pulse. The peak value of

the photocurrent is approximately estimated by the measured current, the pulse dulation, and repetition time. Moreover, the current measured by the source meter includes the dark current as shown in Fig. 8. Therefore, the peak value of the photocurrent corresponding to the peak power can be written as

$$I_{\mathrm{peak}} = (I_{\mathrm{meas}} - I_{\mathrm{dark}}) \times \frac{t_{\mathrm{p}}}{t_{\mathrm{d}}}, \tag{2}$$

where I_{peak}, I_{meas}, and I_{dark} are the peak value of the photocurrent, the measured current, and the dark current, respectively.

Figure 9 shows the peak power density dependence of the photocurrent for both cw and pulse excitation. For the cw excitation (open squares in Fig. 9), which is the case of effective low-power excitation, the photocurrent is defined as a subtracted value by the dark current from a measured value. For the pulse excitation (closed squares in Fig. 9), which is the case of effective high-power excitation, the photocurrent is evaluated from the duty ratio of the pulse laser as mentioned above. The solid line indicates linear absorption. It was found that the photocurrent almost linearly increases with increasing peak power density in a wide range from 10 W/cm^2 to 10 MW/cm^2. The peak power density of 10 MW/cm^2 corresponds to the laser power of ∼10 mW in our study; thus, the photocurrent linearly increases in a power range corresponding to the operation of commercially available PC antennas.

At a power excitation of higher than 10 MW/cm^2, the photocurrent slightly deviated from the linear absorption. This deviation may be induced by a decrease in the absorption coefficient due to saturable absorption. The photocurrent $I(P_{\mathrm{d}})$ as a function of power density P_{d} is proportional to the absorption coefficient and power density of the excitation. Therefore, the photocurrents can be written as $I(P_{\mathrm{d}}) \propto \alpha P_{\mathrm{d}}$. In the case of saturable absorption, the photocurrent can be expressed as

$$I(P_{\mathrm{d}}) \propto \frac{\alpha_0}{1 + \frac{P_{\mathrm{d}}}{P_{\mathrm{s}}}} P_{\mathrm{d}}, \tag{3}$$

where α_0 and P_{s} are the linear absorption coefficient and the saturation intensity, respectively. Using Eq. (3), we estimated the saturation intensity. Figure 10 shows the estimated curve of the photocurrent for $P_{\mathrm{s}} = 90$ MW/cm^2 and the experimental curve for the pulse excitation. Another curve obtained from a reported P_{s}[40,41] of 35 MW/cm^2 for stacked InAs QD layers on an InP substrate with 1.5 μm absorption is also shown

in Fig. 10. The estimated P_s of 90 MW/cm^2 is consistent with the experimental result and comparable to the reported P_s for InAs QDs with 1.5 μm absorption. Therefore, the slight deviation from linear absorption is probably due to the saturable absorption.

4. Conclusions

We have fabricated a photoconductive antenna structure with Er-doped InAs QD layers embedded in strain-relaxed $In_{0.35}Ga_{0.65}As$ layers on a GaAs substrate. The formation of mesa-shaped electrodes was useful for suppressing the dark current for PC antenna structure. Compared with the dark current, the photocurrent was clearly observed and increased as the excitation power increased for both cw and pulse excitation. The relationship between the peak power density and the photocurrent corresponding to the peak power was linear in the wide range from 10 W/cm^2 to 10 MW/cm^2. Above a power density of 10 MW/cm^2, signs of saturable absorption were observed. The estimated saturation intensity was 90 MW/cm^2. Consequently, we have shown that Er-doped InAs QDs embedded in strain-relaxed InGaAs layers have high potential for applications to PC antennas.

Acknowledgment

This work was supported by JPSP KAKENHI Grant Number 26889043.

References

1) M. Tani, K. Sakai, H. Abe, S. Nakashima, H. Harima, M. Hangyo, Y. Tokuda, K. Kanamoto, Y. Abe, and N. Tsukada, Jpn. J. Appl. Phys. **33**, 4807 (1994).
2) K. A. McIntosh, E. R. Brown, K. B. Nichols, O.B. McMahon, W.F. DiNatale, and T. M. Lyszczarz, Appl. Phys. Lett. **67**, 3844 (1995).
3) E. R. Brown, K. A. McIntosh, K. B. Nichols, and C. L. Dennis, Appl. Phys. Lett. **66**, 285 (1995).
4) S. Matsuura, M. Tani, and K. Sakai, Appl. Phys. Lett. **70**, 559 (1997).
5) M. Tani, K. Sakai, and H. Mimura, Jpn. J. Appl. Phys. **36**, 1175 (1997).
6) S. Kono, M. Tani, P. Gu, and K. Sakai, Appl. Phys. Lett. **77**, 4104 (2000).
7) S. Gupta, M. Y. Frankel, J. A. Valdmanis, J. F. Whitaker, G. A. Mourou, F. W. Smith, and A.R. Calawa, Appl. Phys. Lett. **59**, 3276 (1991).
8) S. Gupta, J. F. Whitaker, and G. A. Mourou, IEEE J. Quantum Electron. **28**, 2464 (1992).
9) G. L. Witt, Mater. Sci. Eng. B **22**, 9 (1993).
10) M. Tani, S. Matsuura, K. Sakai, and S. Nakashima, Appl. Phys. Lett. **36**, 7853 (1997).
11) I. S. Gregory, C. Baker, W. R. Tribe, M. J. Evans, H. E. Beere, E. H. Linfield, A. G. Davies, and M. Missous, Appl. Phys. Lett. **83**, 4199 (2003).
12) A. Takazato, M. Kamakura, T. Matsui, J. Kitagawa, and Y. Kadoya, Appl. Phys. Lett. **91**, 011102 (2007).
13) B. Sartorius, H. Roehle, H. Kunzel, J. Bottcher, M. Schlak, D. Stanze, H. Venghaus, and M. Schell, Opt. Express **16**, 9565 (2008).
14) E. H. V. Parker, *The Technology and Physics of Molecular Beam Epitaxy*, Springer, New York 1985. p. 128.
15) S. Gupta, P. K. Bhattacharya, J. Pamulapati, and G. Mourou, Appl. Phys. Lett. **57**, 1543 (1990).
16) M. Shkhotin, E. R. Brown, A. C. Gossard, D. Driscoll, M. Hanson, P. Maker, and R. Muller, Appl. Phys. Lett. **82**, 3116 (2003).
17) A. Schwagmann, Z. Y. Zhao, F. Ospald, H. Lu, D. C. Driscoll, M. P. Hanson, A. C. Gossard, and J. H. Smet, Appl. Phys. Lett. **96**, 141108 (2010).
18) H. Roehlo, H. J. Hensel, J. Bottcher, H. Kunzel, D. Stanze, M. Schell, and B. Sartorius, Opt. Express **18**, 2296 (2010).

19) I. Kostakis, D. Saeedkia, and M. Missous, IEEE Trans. Terahertz Scie. Technol. **2**, 617 (2012).
20) C. Baker, I. S. Gregory, W. R. Tribe, I. V. Bradley, M. J. Evans, M. Withers, P. F. Taday, V. P. Wallace, E. H. Linfield, A. G. Davies, and M. Missous, Appl. Phys. Lett. **83**, 4113 (2003).
21) T. Tanabe, J. Nishizawa, K. Suto, Y. Watanabe, T. Sasaki, and Y. Oyama, Mater. Trans. **18**, 980 (2007).
22) R. J. B. Dietz, R. Wilk, B. Globisch, H. Roehle, D. Stanze, S. Ullrich, S. Schumann, N. Born, M. Koch, B. Sartorius, and M. Schell, J. Infrared Millimeter Terahertz Waves **34**, 231 (2013).
23) R. J. B. Dietz, A. Brahm, A. Velauthapillai, A. Wilms, C. Lammers, B. Globisch, M. Koch, G. Notni, A. T*ü*nnermann, T. G*ö*bel, and M. Schell, J. Infrared Millimeter Terahertz Waves **36**, 60 (2015).
24) K. Murakumo, N. Kumagai, T. Kitada, and T. Isu, Int. Symp. Compound Semiconductors (ISCS2015), 2015, Mo.3.GN1.2.
25) N. Kumagai, K. Murakumo, T. Kitada, and T. Isu, Int. Conf. Modulated Semiconductor Structures (MSS17), 2015, Mo-PM-14.
26) T. Kitada, T. Mukai, T. Takahashi, K. Morita, and T. Isu, J. Cryst. Growth **311**, 1807 (2009).
27) M. G. Alessi, M. Capizzi, A. Bhatti, A. Frova, F. Martelli, P. Frigeri, A. Bosacchi, and S. Franchi. Phys. Rev. B **59**, 7620 (1999).
28) L. Chu, M. Arzberger, G. Bohm, and G. Abstreiter, J. Appl. Phys. **85**, 2355 (1999).
29) J. Z. Wang, Z. M. Wang, Z. G. Wang, Y. H. Chen, and Z. Yang, Phys. Rev. B **61**, 614 (2000).
30) K. Yamaguchi, K. Yujobo, and T. Kaizu, Jpn. J. Appl. Phys. **39**, 1245 (2000).
31) P. B. Joyce, T. J. Krzyzewski, G. R. Bell, T. S. Jones, S. Malik, D. Childs, and R. Murray Phys. Rev. B **62**, 891 (2000).
32) P. B. Joyce, T. J. Krzyzewski, G. R. Bell, T. S. Jones, E. C. Le Ru, and R. Murray, Phys. Rev. B **64**, 235317 (2001).
33) K. Nishi, H. Saito, S. Sugou, and J. S. Lee, Appl. Phys. Lett. **74**, 1111 (1999).
34) V. M. Ustinov, N. A. Maleev, A. E. Zhukov, A. R. Kovsh, A. Yu. Egorov, A. V. Lunev, B. V. Volovik, I. L. Krestnikov, Yu. G. Musikhin, N. A. Bert, P. S. Kop'ev, Zh. I. Alferov, N. N. Ledentsov, and D. Bimberg, Appl. Phys. Lett. **74**,

2815 (1999).

35) A. E. Zhukov, A. R. Kovsh, N. A. Maleev, S. S. Mikhrin, V. M. Ustinov, A. F. Tsatsul'nikov, M. V. Maximov, B. V. Volovik, D. A. Bedarev, Yu. M. Shernyakov, P. S. Kop'ev, Zh. I. Alferov, N. N. Ledentsov, and D. Bimberg, Appl. Phys. Lett. **75**, 1926 (1999).

36) H. Yu, S. Lycett, C. Roberts, and R. Murray, Appl. Phys. Lett. **69**, 4087 (1996).

37) D. A. Yarotski, R. D. Averitt, N. Negre, S. A. Crooker, and A. J. Taylor, J. Opt. Soc. **19**, 1480 (2002).

38) T. Kitada, T. Takahashi, H. Ueyama, K. Morita, and T. Isu, J. Cryst. Growth **323**, 241 (2011).

39) T. Kitada, H. Ueyama, K. Morita, and T. Isu, J. Cryst. Growth **378**, 485 (2013).

40) T. Isu, J. Inoue, K. Akahane, H. Sotobayashi, and M. Tsuchiya, Proc. SPIE **6393**, 639309 (2006).

41) J. Inoue, T. Isu, K. Akahane, and M. Tsuchiya, Appl. Phys. Lett. **89**, 151117 (2006).

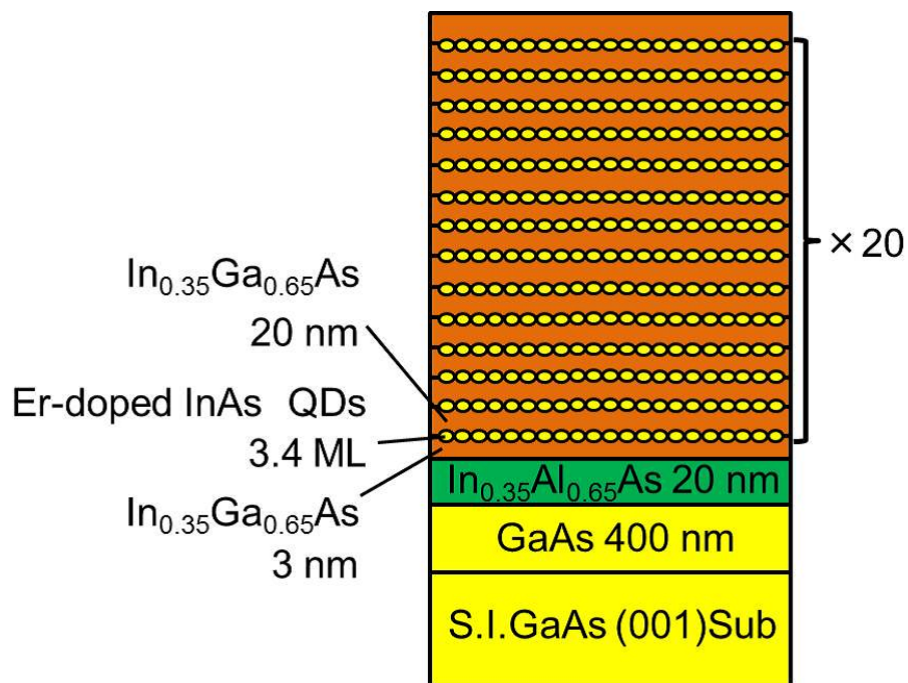

Fig. 1. (Color online) Stacking structure of Er-doped InAs QD layers embedded in strain-relaxed InGaAs layers on GaAs substrate.

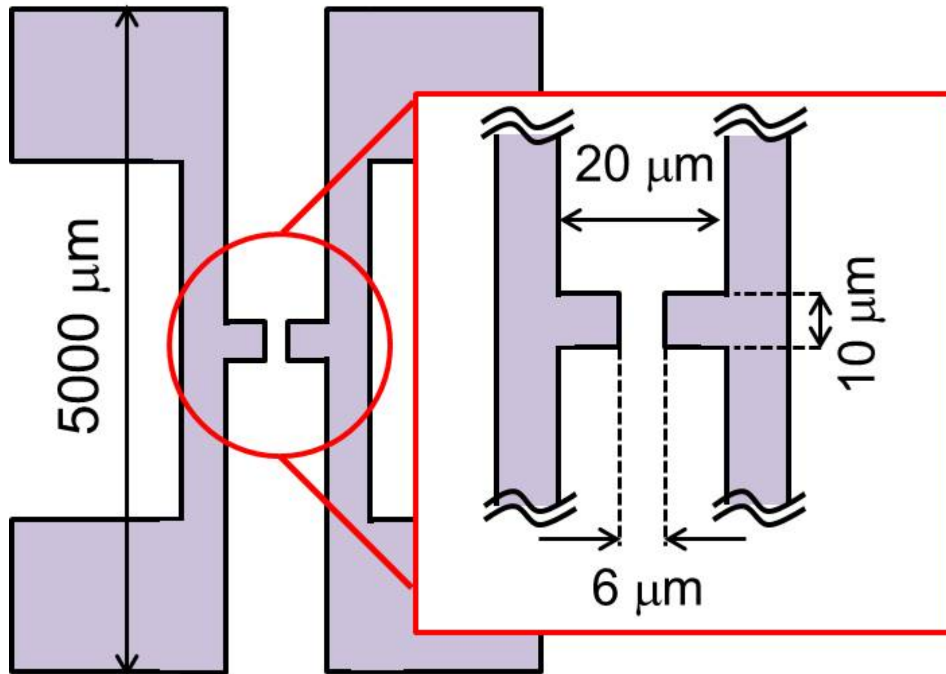

Fig. 2. (Color online) Schematic pattern of dipole antenna for PC antenna structure and the enlargement of its antenna gap.

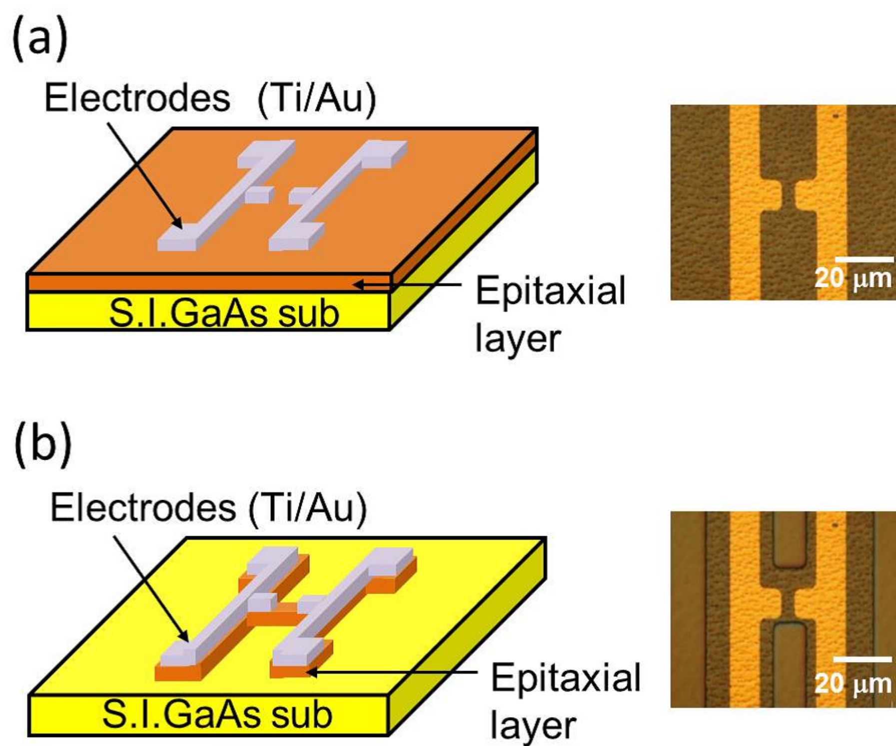

Fig. 3. (Color online) Schematic illustrations of PC antenna and enlarged image of the antenna gap (a) without and (b) with the formation of mesa-shaped electrodes.

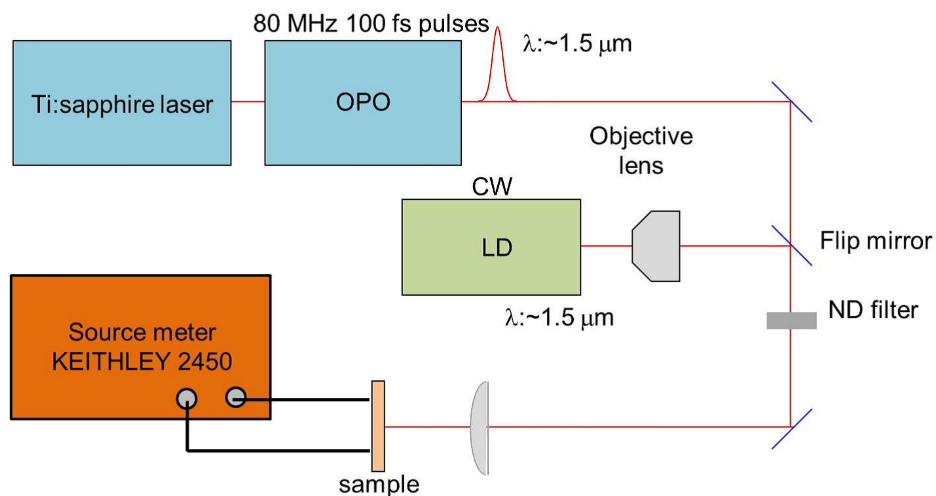

Fig. 4. (Color online) Schematic diagram of the setup for photocurrent measurement in this study.

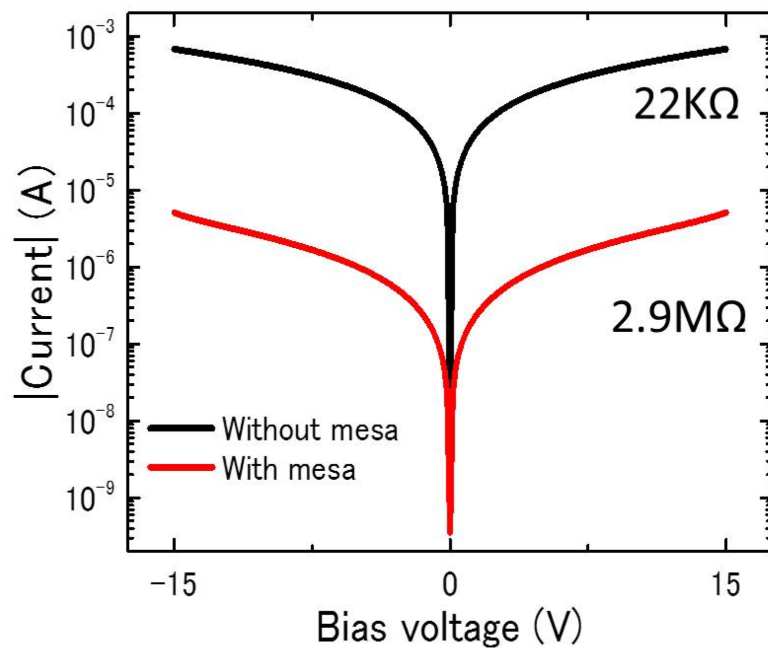

Fig. 5. (Color online) I-V characteristics of dark current with and without the formation of mesa-shaped electrodes.

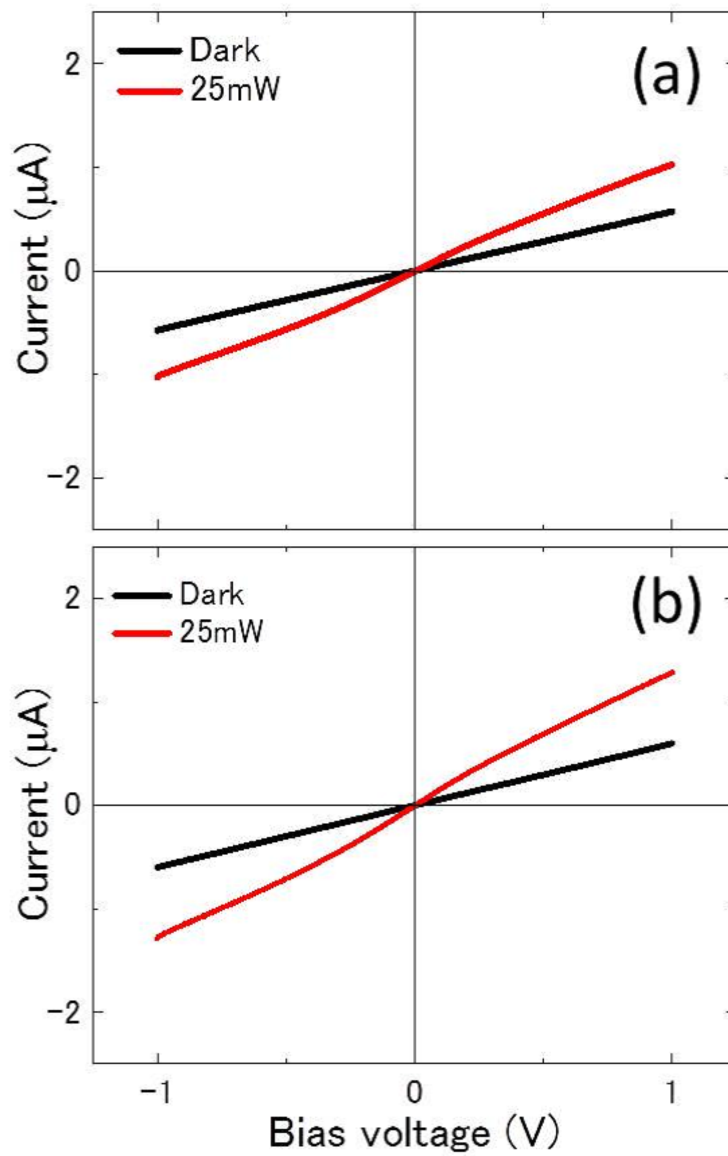

Fig. 6. (Color online) I-V characteristics under dark current and photocurrent with (a) cw excitation and (b) pulse excitation of 1.5 μm.

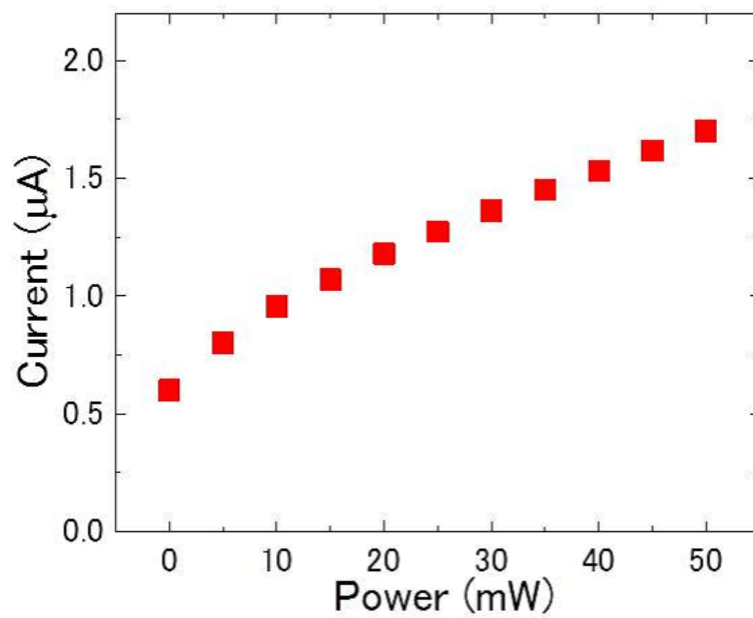

Fig. 7. (Color online) Excitation power dependence of photocurrent with pulse excitation at a wavelength of 1.5 μm.

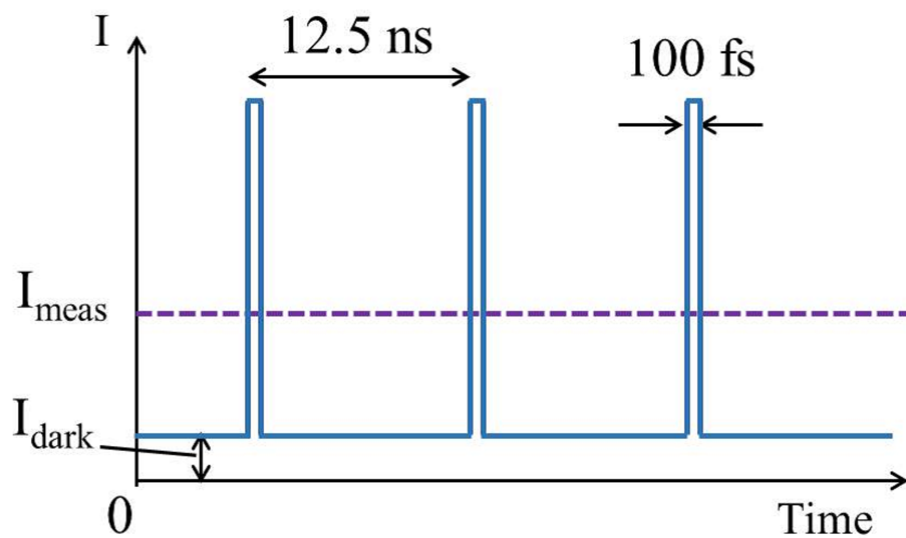

Fig. 8. (Color online) Schematic diagram for relationship among I_{meas}, and I_{dark} for pulse excitation.

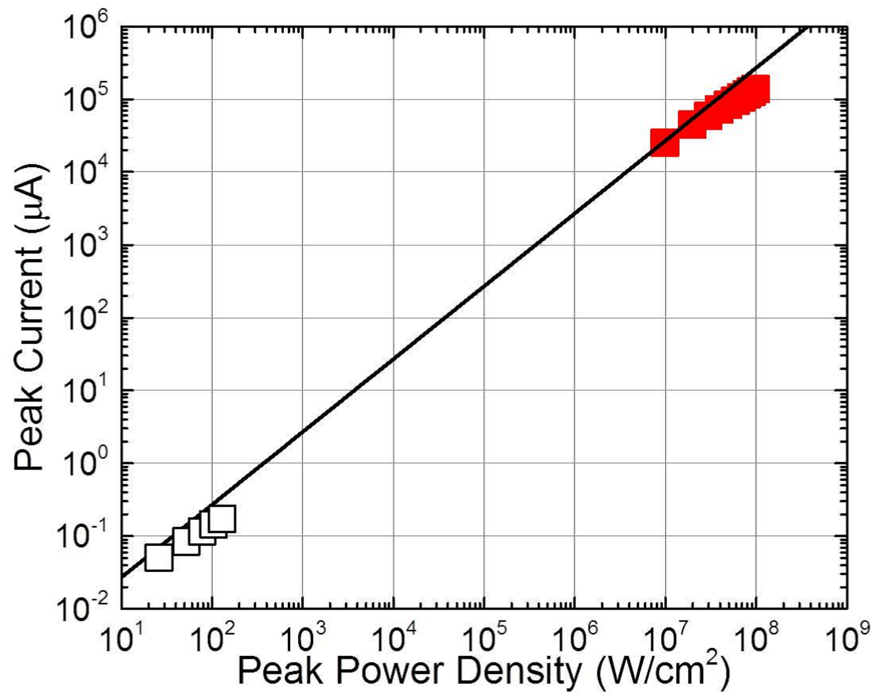

Fig. 9. (Color online) Peak power density dependence of peak current for cw and pulse excitation. Open squares and closed squares are results of the photocurrent for the cw excitation and pulse excitation, respectively. The solid line indicates linear absorption.

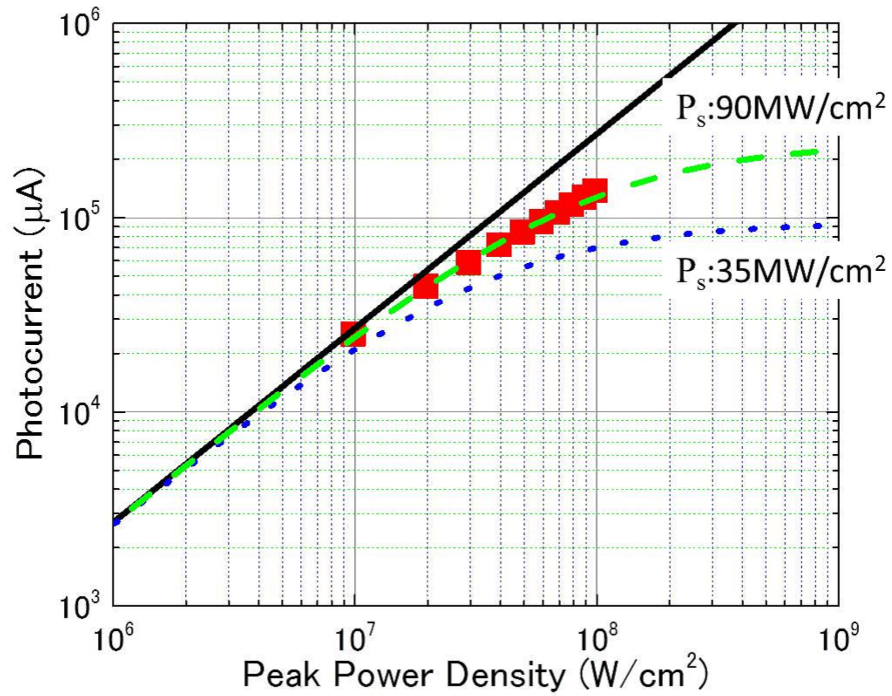

Fig. 10. (Color online) Estimated curves of photocurrent with assumed saturation intensity of 35[40,41] and 90 MW/cm^2. The dotted and dashed lines represent 35 and 90 MW/cm^2, respectively. The solid line represents linear absorption. Closed squares represent experimental results (already shown in Fig. 9).